Glycine *N*-methyltransferase deletion in mice diverts carbon flux from gluconeogenesis to pathways that utilize excess methionine cycle intermediates

Received for publication, February 21, 2018, and in revised form, May 17, 2018 Published, Papers in Press, June 11, 2018, DOI 10.1074/jbc.RA118.002568

Curtis C. Hughey[‡1], Elijah Trefts[‡], Deanna P. Bracy[‡§], Freyja D. James[‡§], E. Patrick Donahue[‡], and David H. Wasserman[‡§]

From the [‡]Department of Molecular Physiology and Biophysics and the [§]Mouse Metabolic Phenotyping Center, Vanderbilt University, Nashville, Tennessee 37232

Edited by John M. Denu

Glycine *N*-methyltransferase (GNMT) is the most abundant liver methyltransferase regulating the availability of the biological methyl donor, *S*-adenosylmethionine (SAM). Moreover, GNMT has been identified to be down-regulated in hepatocellular carcinoma (HCC). Despite its role in regulating SAM levels and association of its down-regulation with liver tumorigenesis, the impact of reduced GNMT on metabolic reprogramming before the manifestation of HCC has not been investigated in detail. Herein, we used $^{2}H/^{13}C$ metabolic flux analysis in conscious, unrestrained mice to test the hypothesis that the absence of GNMT causes metabolic reprogramming. GNMT-null (KO) mice displayed a reduction in blood glucose that was associated with a decline in both hepatic glycogenolysis and gluconeogenesis. The reduced gluconeogenesis was due to a decrease in liver gluconeogenic precursors, citric acid cycle fluxes, and anaplerosis and cataplerosis. A concurrent elevation in both hepatic SAM and metabolites of SAM utilization pathways was observed in the KO mice. Specifically, the increase in metabolites of SAM utilization pathways indicated that hepatic polyamine synthesis and catabolism, transsulfuration, and *de novo* lipogenesis pathways were increased in the KO mice. Of note, these pathways utilize substrates that could otherwise be used for gluconeogenesis. Also, this metabolic reprogramming occurs before the well-documented appearance of HCC in GNMT-null mice. Together, these results indicate that GNMT deletion promotes a metabolic shift whereby nutrients are channeled away from glucose formation toward pathways that utilize the elevated SAM.

Hepatocellular carcinoma (HCC)[2] continues to be a leading form of cancer worldwide (1). This is partly attributable to a rise in nonalcoholic fatty liver disease, an independent risk factor for developing HCC (2, 3). It is notable that reduced liver glycine *N*-methyltransferase (GNMT) is common to both nonalcoholic fatty liver disease and HCC (4–7). A causal role for GNMT in these liver diseases is supported by studies showing that GNMT-null mice develop liver steatosis and HCC at 3 and 8 months of age, respectively (8). GNMT transfers a methyl group from *S*-adenosylmethionine (SAM), the primary biological methyl donor, to glycine, forming sarcosine and *S*-adenosylhomocysteine (9). Given that GNMT is the most abundant hepatic methyltransferase, it is key in regulating SAM availability for a myriad of processes, including transmethylation linked to the pathogenesis of HCC (9).

In addition to changes in SAM-mediated transmethylation, a hallmark of cancer is metabolic reprogramming, which refers to the enhanced or suppressed flux of nutrients through metabolic pathways as a result of mutations and/or other factors (10). A classic example of tumor metabolic reprogramming often observed is an increase in cancer cell glycolysis termed the Warburg effect (11). This atypical metabolic phenotype is thought to provide energetic support for the biosynthetic demand of tumorigenesis (12). Indeed, HCC often displays an accelerated rate of glycolytic flux (13). However, the liver is unique, given it has a high capacity for both glucose utilization and formation. As such, a reduction in hepatic gluconeogenesis may spare substrate for glycolytic flux and promote a metabolic environment that supports HCC (14).

GNMT is abundant in the highly gluconeogenic periportal region of the liver, and SAM may be catabolized to the gluconeogenic precursors, succinate and pyruvate (15). Additionally, liver GNMT activity is increased by glucagon, a stimulator of liver gluconeogenesis (16). The studies presented here test the implications of GNMT deletion on gluconeogenic flux. It was hypothesized that the loss of GNMT and dysregulated liver SAM utilization would be associated with impaired hepatic gluconeogenesis. $^{2}H/^{13}C$ metabolic flux analysis (MFA) deter-

This work was supported by NIDDK, National Institutes of Health, Grants DK050277 and DK054902 (to D. H. W.) and a Diabetes Canada Postdoctoral Fellowship (to C. C. H.). The authors declare that they have no conflicts of interest with the contents of this article. The content is solely the responsibility of the authors and does not necessarily represent the official views of the National Institutes of Health.

This article contains Table S1 and Fig. S1.

[1] To whom correspondence should be addressed: Dept. of Molecular Physiology and Biophysics, Vanderbilt University, 823 Light Hall, 2215 Garland Ave., Nashville, TN 37232. Tel.: 615-343-0580; E-mail: curtis.hughey@vanderbilt.edu.

[2] The abbreviations used are: HCC, hepatocellular carcinoma; 5-mC, 5-methylcytosine; ACC, acetyl-CoA carboxylase; ACLY, ATP-citrate lyase; ALT, alanine aminotransferase; AST, aspartate aminotransferase; CAC, citric acid cycle; ETS, maximal respiration by the electron transport system; GNMT, glycine *N*-methyltransferase; GSS, glutathione synthetase; LEAK, futile oxygen consumption; MFA, metabolic flux analysis; MTA, 5-methylthioadenosine; NNMT, nicotinamide *N*-methyltransferase; PC, pyruvate carboxylase; PEPCK, phosphoenolpyruvate carboxykinase; PVDF, polyvinylidene difluoride; PYGL, glycogen phosphorylase; SAM, *S*-adenosylmethionine; KO, knockout; BisTris, 2-[bis(2-hydroxyethyl)amino]-2-(hydroxymethyl) propane-1,3-diol; TAN, total adenine nucleotide.

Table 1
Biometric characteristics in glycine *N*-methyltransferase-null mice

Body composition data are from glycine *N*-methyltransferase KO mice and WT littermates with free access to food and water. Data are mean ± S.E. for $n = 21–25$ mice/genotype. In a separate cohort of mice ("liver characteristics"), body weight, liver weight, and liver/body ratio were determined in WT and KO littermates following an 8-h fast. Data are for mean ± S.E. for $n = 8–10$ mice/genotype. Arterial plasma non-esterified fatty acids were obtained from catheterized WT and KO littermates undergoing stable isotope infusions 7 h and 40 min following food and water. Data are mean ± S.E. for $n = 7–11$ mice/genotype. Arterial plasma insulin and glucagon were obtained from catheterized KO and WT littermates undergoing stable isotope infusions 8 h following food and water withdrawal. For fasting studies, food and water were withdrawn during the first hour of the light cycle. Data are mean ± S.E. for $n = 7–11$ mice/genotype. Biometric characteristics were collected for male mice only. *, $p < 0.05$ *versus* WT.

Parameters	WT	KO
Body composition		
Body weight (g)	25.4 ± 0.4	23.5 ± 0.4*
Lean mass (g)	18.2 ± 0.2	16.8 ± 0.3*
Fat mass (g)	1.9 ± 0.1	1.9 ± 0.1
Liver characteristics		
Body weight (g)	23.9 ± 0.3	23.4 ± 1.1
Liver weight (g)	1.0 ± 0.0	1.6 ± 0.1*
Liver/body weight (%)	4.3 ± 0.1	6.9 ± 0.4*
Plasma hormones and metabolites		
Plasma insulin (pmol/liter)	106 ± 24	90 ± 17
Plasma glucagon (pmol/liter)	17 ± 5	13 ± 4
Plasma non-esterified fatty acids (mmol/liter)	0.90 ± 0.04	0.94 ± 0.09

mined hepatic nutrient fluxes in conscious, unrestrained GNMT-knockout (KO) mice and WT littermates under post-absorptive conditions at 3 months of age. KO mice of this age were chosen, as this allows for the identification of metabolic reprogramming before the onset of HCC, which occurs as early as 8 months of age in mice lacking GNMT (8, 17, 18). The results show that lack of GNMT reduces gluconeogenesis from phosphoenolpyruvate. Molecular and qualitative metabolomic analyses suggest that this is driven by the channeling of gluconeogenic precursors away from glucose formation to processes that act to counter the elevated SAM in KO mice. These processes include polyamine synthesis and catabolism, GSH synthesis from transsulfuration, and lipogenesis.

Results

GNMT KO mice display hepatomegaly

In a large cohort of mice, the KO group exhibited a small but significant reduction in the body weight of mice fed *ad libitum* (Table 1). This was due to decreased lean mass (Table 1). In a smaller, independent cohort of 8-h-fasted mice, the alteration in body weight was not detectable (Table 1). KO mice exhibited a 1.6-fold increase in liver weight and liver/body weight ratio (Table 1). Arterial plasma insulin, glucagon, and nonesterified fatty acids were comparable between genotypes under post-absorptive conditions (Table 1).

GNMT KO mice exhibit liver methionine cycle dysregulation and steatosis

Loss of GNMT, a regulator of SAM (Fig. 1*A*), was confirmed in KO mice via immunoblotting (Fig. 1*B*). Liver methionine cycle intermediates, methionine and SAM, were elevated in KO mice (Fig. 1*C*). Methionine precursor, betaine, was also higher in KO mice (Fig. 1*C*). Coincident with the elevated SAM concentrations in KO mice was a reduction in global DNA methylation marker (5-methylcytosine; 5-mC) (Fig. 1*D*). The activities of liver enzymes, alanine (ALT) and aspartate (AST) aminotransferase, were higher in KO mice (Fig. 1, *E* and *F*). KO mice showed a 2-fold increase in liver triacylglycerides (Fig. 1*G*). Collagen as a percentage of tissue area was similar between groups (Fig. 1*H*). The percentage of Ki67-positive nuclei was comparable between genotypes, indicating no change in cell proliferation and that mice were pretumorigenic (Fig. 1*I*).

Altered glucose homeostasis in GNMT KO mice

The current study tested the hypothesis that alterations in liver glucose formation (Fig. 2*A*) were regulated by GNMT-mediated transmethylation. KO mice exhibited lower arterial blood glucose throughout the experiment (Fig. 2*B*). This was accompanied by a decline in endogenous glucose production in KO mice (V_{EndoRa}; Fig. 2*C*). Glycogenolysis, flux of glycogen to glucose 6-phosphate (V_{PYGL}), was lower (Fig. 2*C*). Total gluconeogenic flux (V_{Aldo}) was reduced in KO mice as a result of a decline in phosphoenolpyruvate to glyceraldehyde 3-phosphate (V_{Enol}; Fig. 2*C*). The lower glycogenolysis in KO mice was associated with higher glycogen (Fig. 2*D*) and glucose 6-phosphate (Fig. 2*F*). Hepatic gluconeogenic metabolites were also assessed. KO mice had reduced glyceraldehyde 3-phosphate and phosphoenolpyruvate (Fig. 2*F*).

Impaired citric acid cycle–related fluxes in GNMT KO mice

The generation of phosphoenolpyruvate for gluconeogenesis is linked to the entry and exit of substrate into and from the citric acid cycle (CAC) (Fig. 3*A*). Pyruvate recycling, modeled as flux of phosphoenolpyruvate to pyruvate (V_{PK+ME}), was reduced in KO compared with WT mice (Fig. 3*B*). The flux of nonphosphoenolpyruvate-derived, unlabeled anaplerotic substrate to pyruvate (V_{UAS}; modeled as unlabeled lactate to pyruvate) was reduced in KO mice (Fig. 3*B*). Anaplerotic fluxes, modeled as V_{PC} (flux from pyruvate to oxaloacetate) and V_{PCC} (flux from propionyl-CoA to succinyl-CoA), were lower in the KO mice (Fig. 3*B*). This was associated with a reduction in pyruvate carboxylase (PC) protein (Fig. 3*C*). Cataplerosis (V_{PCK}; modeled as flux from oxaloacetate to phosphoenolpyruvate) was reduced in KO mice (Fig. 3*B*) despite a ~3–4-fold increase in phosphoenolpyruvate carboxykinase (PEPCK) (Fig. 3*C*). KO mice displayed a decline in CAC fluxes (V_{CS} and V_{SDH}) (Fig. 3*B*).

Qualitative metabolomics was performed on liver tissue to enrich the dynamic insight provided by $^{2}H/^{13}C$ MFA. Pyruvate was reduced in the KO mice (Fig. 3*D*). Hepatic CAC intermediates (citrate, aconitate, and succinylcarnitine) were increased in KO mice compared with WT (Fig. 3*D*). Amino acids provide anaplerotic and gluconeogenic substrates following deamination (19). Aminotransferases mediate the transfer of the amino group to α-ketoglutarate, among other intermediates, forming glutamate (19). In agreement with the increased AST and ALT activity (Fig. 1, *E* and *F*), livers from KO mice had higher glutamate, and many of the measured amino acids were reduced in the livers of KO mice (Fig. 3*E*).

Compromised energy metabolism in livers of KO mice

Glucose synthesis from CAC-derived sources is energetically demanding (20), making ATP and its provision (Fig. 4*A*) impor-

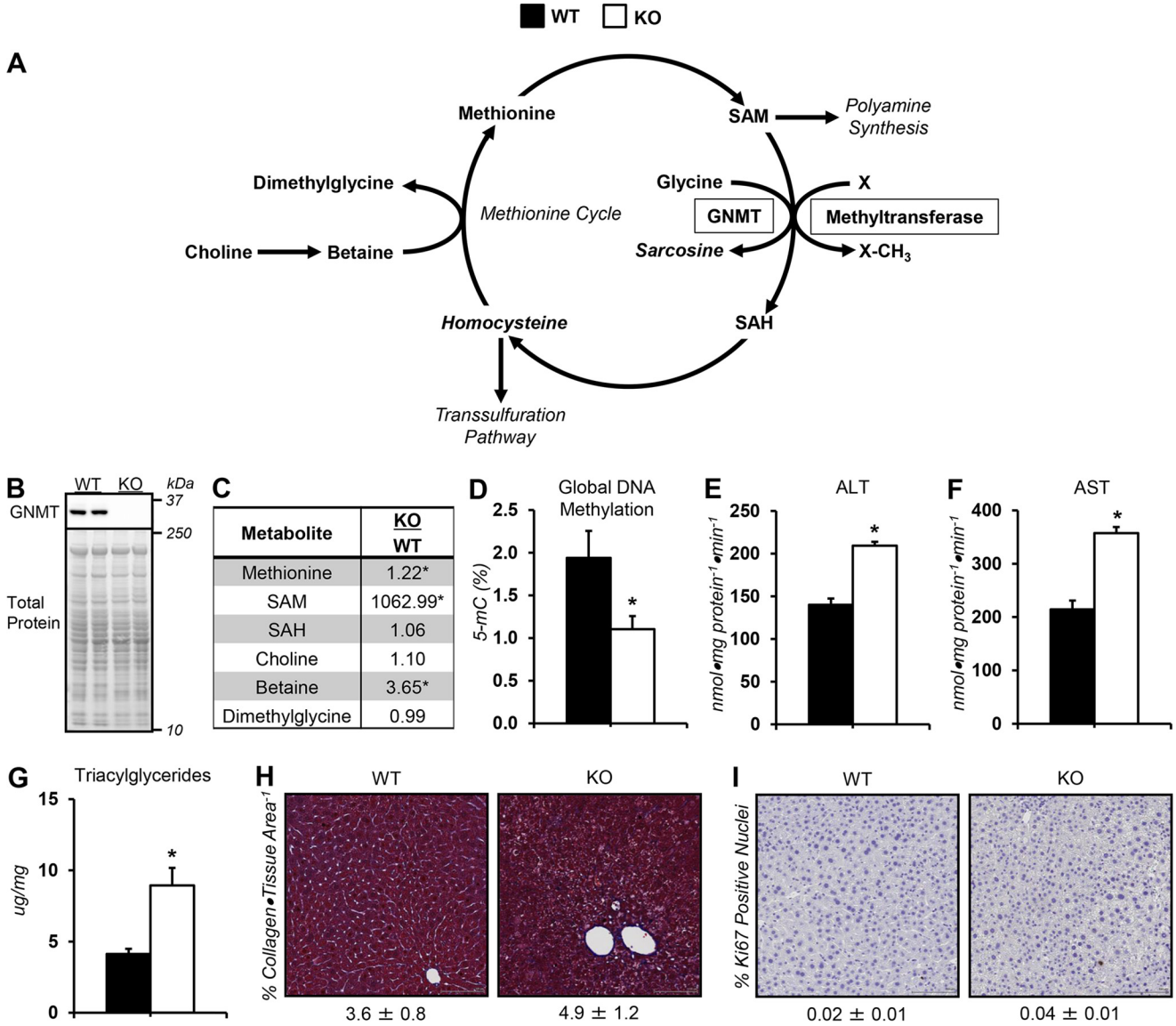

Figure 1. Dysregulated methionine cycle metabolism in glycine *N*-methyltransferase knockout mice. *A*, *schematic representation* of select reactions, enzymes, and metabolites associated with one-carbon metabolism. *Italicized* metabolites were not measured. Enzymes are enclosed in *boxes*. *B*, representative liver GNMT immunoblots from WT mice and KO mice exhibiting a whole-body deletion of GNMT. *C*, liver methionine cycle–related metabolites: methionine, SAM, *S*-adenosylhomocysteine (*SAH*), choline, betaine, and dimethylglycine. *D*, 5-methylcytosine relative to total DNA (*5-mC* %) from liver. Liver ALT (*E*) and AST (*F*) aminotransferase activity are shown. *G*, liver triacylglycerides. *H*, percentage of collagen area per tissue area as determined by Masson's trichrome blue stain and representative images (×20 magnification) for WT and KO mice. *I*, percentage of Ki67-positive nuclei and representative images (×20 magnification) for WT and KO mice. Data are mean ± S.E. (*error bars*). $n = 6–9$ mice/group. *, $p < 0.05$ *versus* WT.

tant for this anabolic process. Liver ATP was lower in KO mice compared with WT mice (Fig. 4*B*). Liver ADP was ~3.5-fold higher in the KO group (Fig. 4*B*). This prompted an increase in total adenine nucleotide (TAN) in KO mice (Fig. 4*B*). Moreover, energy charge and ADP/ATP were decreased and increased, respectively, in KO mice (Fig. 4*B*).

The increased ADP corresponded to oxidative phosphorylation dysfunction in KO mice. Routine respiration was lower in KO mice (Fig. 4*C*). Futile respiration (LEAK) relative to routine respiration and maximal respiration by the electron transport system (ETS) was greater in KO mice (Fig. 4*C*). Routine respiration relative to ETS was lower in KO mice (Fig. 4*C*).

In the absence of GNMT, the activities of other methyltransferases may increase to normalize SAM (21). Nicotinamide *N*-methyltransferase (NNMT) transfers a methyl group to nicotinamide, forming 1-methylnicotinamide (Fig. 4*D*). Nicotinamide and 1-methylnicotinamide are decreased and increased, respectively, in KO mice (Fig. 4*E*). This suggests that NNMT activity is increased. Nicotinamide mononucleotide and NAD^+ were lower in livers from KO mice (Fig. 4*E*). Thus, lower NAD^+ salvage reduces NADH for ATP synthesis.

Elevated SAM increases polyamine synthesis, polyamine catabolism, and transsulfuration in KO mice

The redirection of SAM to polyamine synthesis is reflected by elevated liver putrescine, spermidine, and 5-methylthioadenosine (MTA) in KO mice and reduced ornithine (Fig. 5*B*). Liver adenine, a product of MTA catabolism, was higher in KO mice (Fig. 5*B*).

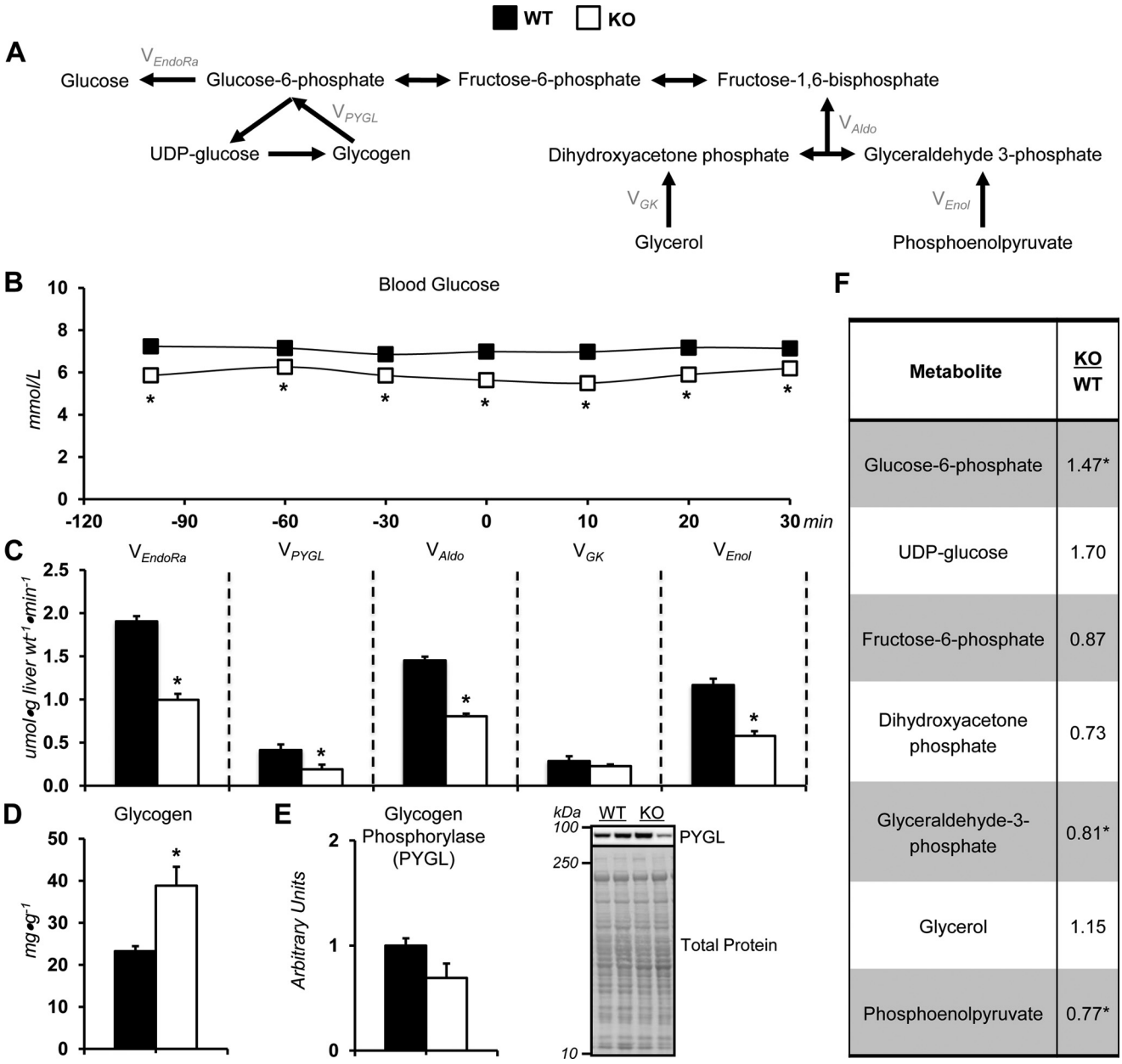

Metabolite	KO / WT
Glucose-6-phosphate	1.47*
UDP-glucose	1.70
Fructose-6-phosphate	0.87
Dihydroxyacetone phosphate	0.73
Glyceraldehyde-3-phosphate	0.81*
Glycerol	1.15
Phosphoenolpyruvate	0.77*

Figure 2. Altered glucose producing fluxes in glycine *N*-methyltransferase knockout mice. *A*, *schematic representation* of select metabolites and fluxes (*highlighted* in *gray*) from $^{2}H/^{13}C$ metabolic flux analysis contributing to endogenous glucose production. *B*, a time course of fasting arterial blood glucose concentration before and during acquisition of plasma for $^{2}H/^{13}C$ metabolic flux analysis in WT and glycine *N*-methyltransferase KO mice. *C*, model-estimated, absolute nutrient fluxes normalized to liver weight (μmol·g liver weight^{-1}·min^{-1}) in mice for endogenous glucose production (V_{EndoRa}), flux from glycogen to glucose 6-phosphate (V_{PYGL}), flux from dihydroxyacetone phosphate and glyceraldehyde 3-phosphate (V_{Aldo}), flux from glycerol to dihydroxyacetone phosphate (V_{GK}; hexose units), and flux from phosphoenolpyruvate to glyceraldehyde-3-phosphate (V_{Enol}; hexose units). *D*, liver glycogen concentration. *E*, liver PYGL as determined by immunoblotting and representative immunoblot. *F*, glycogen- and gluconeogenesis-related metabolites: glucose 6-phosphate (*G6P*), UDP-glucose, fructose 6-phosphate (*F6P*), dihydroxyacetone phosphate (*DHAP*), glyceraldehyde 3-phosphate (*GAP*), glycerol, and phosphoenolpyruvate (*PEP*). Data are mean ± S.E. (*error bars*). $n = 6–11$ mice/group. *, $p < 0.05$ *versus* WT.

Polyamine homeostasis is also influenced by a catabolic pathway involving spermidine acetylation, which allows for the resynthesis of putrescine and may assist in SAM utilization (22). N^1-Acetylspermidine was higher in KO mice (Fig. 5*B*). Hepatic acetylcarnitine was comparable between genotypes (Fig. 5*B*). However, ATP-citrate lyase (ACLY) protein was increased in KO mice (Fig. 5*C*). Given that ACLY cleaves citrate to acetyl-CoA and oxaloacetate, this reaction may lower SAM in KO mice by providing substrate for spermidine acetylation (Fig. 5*A*).

The generation of acetyl-CoA from citrate may also promote liver steatosis in KO mice via *de novo* lipogenesis and/or the inhibition of lipid oxidation. Hepatic malonylcarnitine was increased in KO mice (Fig. 5*B*). Acetyl-CoA carboxylase (ACC) was higher in livers form KO mice (Fig. 5*D*). Livers from KO mice had greater carnitine and lower long-chain acylcarnitines (Table 2). Liver triacylglyceride accumulation in KO mice has been reported to be the result of a compensatory increase in phosphatidylethanolamine methyltransferase activity in response to elevated SAM availability (21). This is supported by data in Table S1.

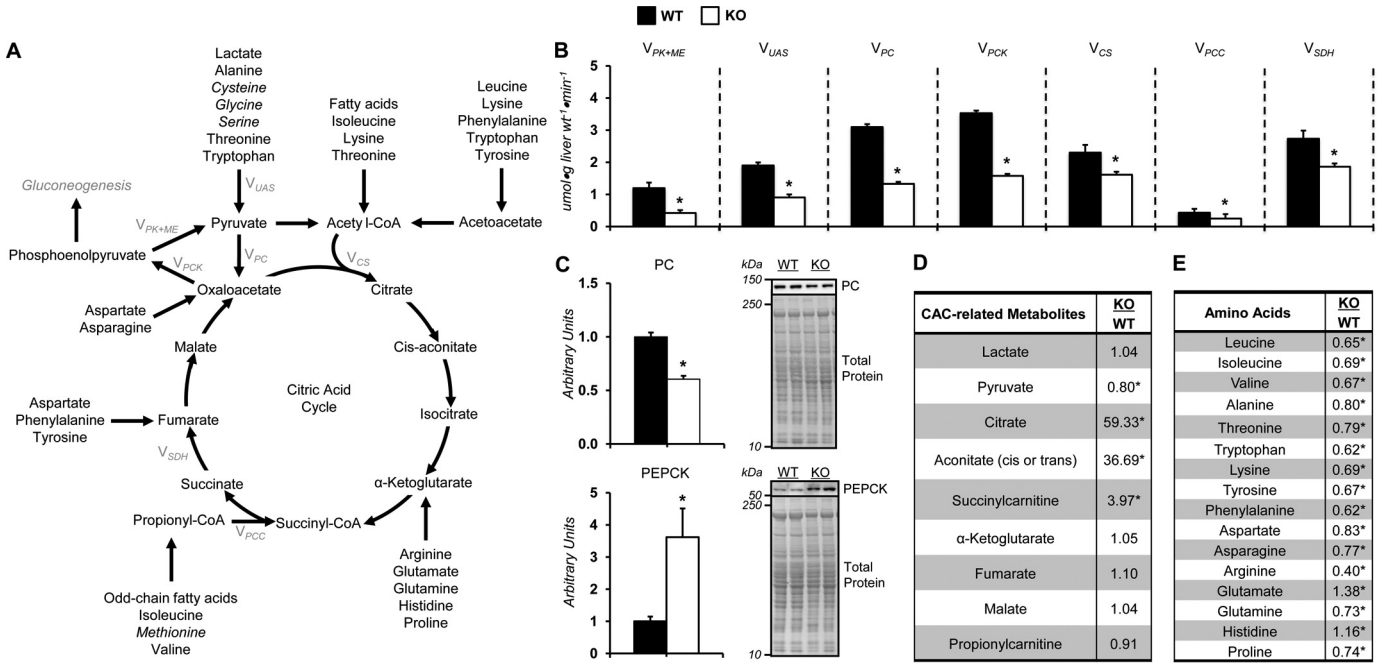

CAC-related Metabolites	KO/WT
Lactate	1.04
Pyruvate	0.80*
Citrate	59.33*
Aconitate (cis or trans)	36.69*
Succinylcarnitine	3.97*
α-Ketoglutarate	1.05
Fumarate	1.10
Malate	1.04
Propionylcarnitine	0.91

Amino Acids	KO/WT
Leucine	0.65*
Isoleucine	0.69*
Valine	0.67*
Alanine	0.80*
Threonine	0.79*
Tryptophan	0.62*
Lysine	0.69*
Tyrosine	0.67*
Phenylalanine	0.62*
Aspartate	0.83*
Asparagine	0.77*
Arginine	0.40*
Glutamate	1.38*
Glutamine	0.73*
Histidine	1.16*
Proline	0.74*

Figure 3. Impaired citric acid cycle–related fluxes *in vivo* in glycine *N*-methyltransferase knockout mice. *A*, schematic representation of select enzymes, metabolites, and fluxes (*highlighted* in *gray*) from $^{2}H/^{13}C$ metabolic flux analysis associated with citric acid cycle metabolism, anaplerosis, and cataplerosis. *Italicized* metabolites are intimately associated with SAM homeostasis and are provided in other figures. *B*, model-estimated, absolute nutrient fluxes normalized to liver weight (μmol·g liver weight^{-1}·min^{-1}) in post-absorptive glycine *N*-methyltransferase KO and WT mice for contribution of pyruvate kinase and malic enzyme to pyruvate (V_{PK+ME}), flux from nonphosphoenolpyruvate-derived, unlabeled anaplerotic substrate to pyruvate (V_{UAS}), anaplerotic flux as modeled by pyruvate to oxaloacetate (V_{PC}), cataplerotic flux modeled as oxaloacetate to phosphoenolpyruvate (V_{PCK}), flux from oxaloacetate and acetyl-CoA to citrate (V_{CS}), anaplerotic flux as modeled by propionyl-CoA to succinyl-CoA (V_{PCC}), and flux from succinyl-CoA to oxaloacetate (V_{SDH}). *C*, liver cytosolic PEPCK and PC as determined by immunoblotting and representative immunoblot. The total protein loading control image for PC is the same as that used for PYGL in Fig. 2*E*, given that the immunoblots were performed on the same PVDF membrane. *D*, liver CAC and related metabolites: lactate, pyruvate, citrate, aconitate, succinylcarnitine, α-ketoglutarate, fumarate, malate, and propionylcarnitine. *E*, hepatic amino acids: leucine, isoleucine, valine, alanine, threonine, tryptophan, lysine, tyrosine, phenylalanine, aspartate, asparagine, arginine, glutamate, glutamine, histidine, and proline. Data are mean ± S.E. (*error bars*). $n = 6–11$ mice/group. *, $p < 0.05$ *versus* WT.

Transsulfuration is up-regulated in KO mice, as reflected by reduced serine and increased cystathionine and cysteine (Fig. 5*B*). Cysteine is a precursor for GSH (Fig. 5*A*). KO mice displayed lower glycine and higher GSH (Fig. 5*B*). GSH synthetase (GSS) protein was higher in liver of KO mice (Fig. 5*E*). Also, the expanded GSH pool in KO mice was associated with greater 4-hydroxynonenal-GSH (*GS-HNE*; Fig. 5*B*). Thus, the greater transsulfuration in KO mice is linked to altered liver redox status.

Discussion

Metabolic reprogramming such as the increased glycolysis (*i.e.* Warburg effect) that occurs in cancer supports the nutrient and energetic requirements of tumorigenesis (10–12). In the liver, a reduction in gluconeogenesis may also promote cancer via the sparing of nutrient and energy resources (14, 23, 24). Loss of GNMT has been implicated in the pathogenesis of HCC (6–8, 17). The extent to which the absence of GNMT results in metabolic reprogramming and altered glucose handling remains unanswered. The studies presented here tested the role of GNMT in regulating glucose formation and intermediary metabolism using $^{2}H/^{13}C$ MFA and qualitative metabolomics in mutant mice. Of note, the metabolomics utilized provides relative differences in metabolite levels between genotypes. This approach limits the information that could be obtained from quantitative metabolite values and the ability to make comparisons with metabolite concentrations in the literature.

KO mice showed a profound increase in liver SAM. This was associated with reduced endogenous glucose production owing to impairments in nutrient flux at multiple sites (glycogenolysis, gluconeogenesis, and oxidative metabolism). The changes in glucose metabolism were accompanied by an increase in lipid accumulation, polyamine synthesis and breakdown, and transsulfuration in KO mice. These results show that GNMT KO results in metabolic reprogramming whereby carbons are redirected from the gluconeogenic pathway to biosynthetic pathways that utilize SAM (Fig. 6).

Glucose formation in the livers of KO mice

Nutrient flux, energy state, and redox potential are interconnected such that an alteration in one of these variables may influence another. GNMT and SAM hold potential in regulating multiple aspects of the liver's metabolic network that could influence glucose control. In agreement with previous studies (21, 25), blood glucose was reduced in fasting KO mice. The studies here show that the lower arterial glucose was accompanied by decreased endogenous glucose production (V_{EndoRa}). Impaired glycogenolysis has been hypothesized as a mechanism for the lower blood glucose, given that liver glycogen accumulates in GNMT-deficient mice (25, 26). The present study also identified an increase in hepatic glycogen content in KO mice. This is consistent with decreased fusion of autophagic vacuoles with lysosomes as well as a decline in expression of liver α-glu-

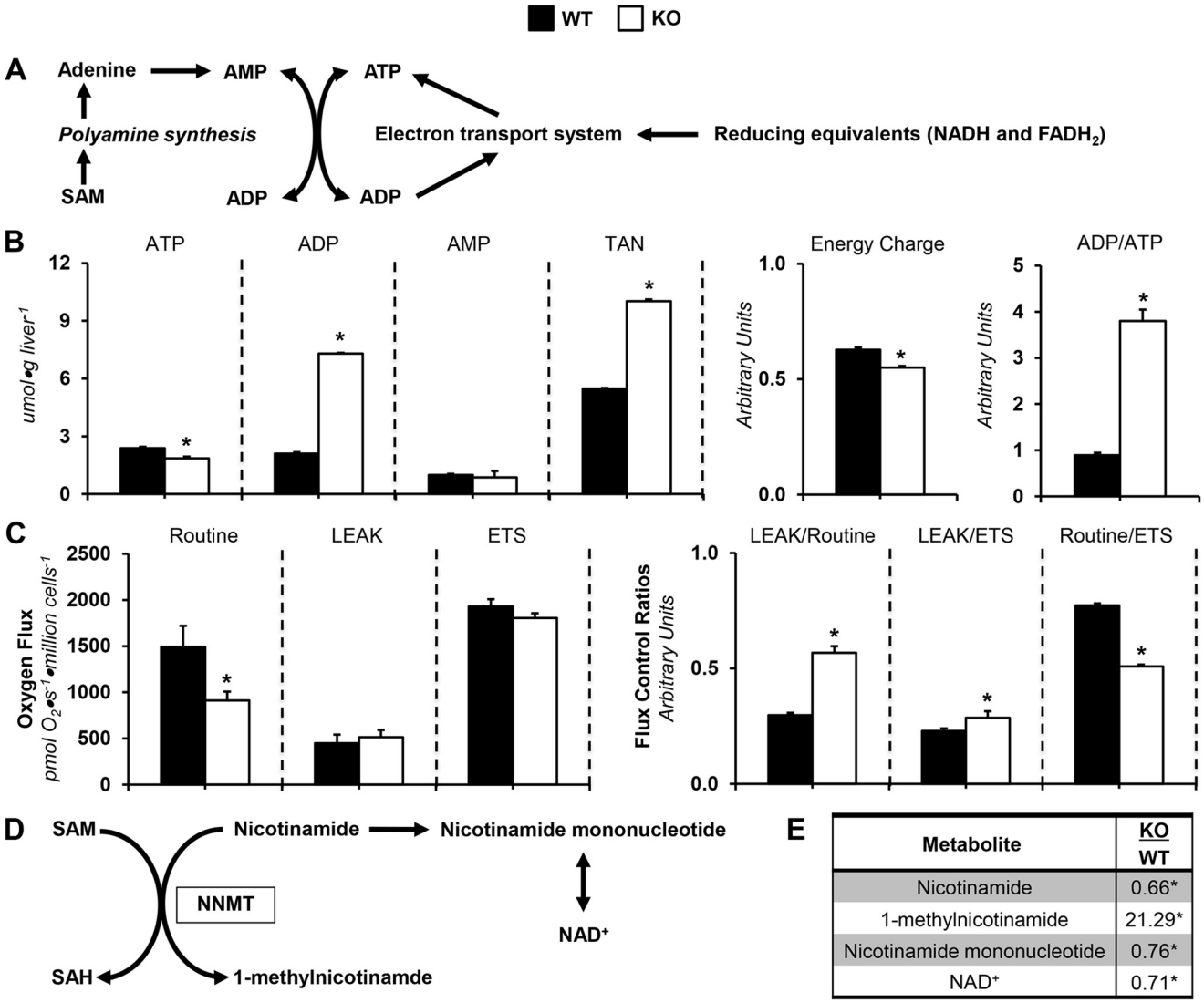

E

Metabolite	KO / WT
Nicotinamide	0.66*
1-methylnicotinamide	21.29*
Nicotinamide mononucleotide	0.76*
NAD^+	0.71*

Figure 4. Dysregulated energy metabolism in glycine *N*-methyltransferase knockout mice. *A*, schematic representation of select metabolites and pathways related to energy homeostasis. *B*, hepatic adenine purine nucleotides ATP, ADP, AMP, and TAN pool (TAN = ATP + ADP + AMP) from glycine *N*-methyltransferase KO and WT mice. Energy state indexes energy charge ([ATP + 0.5·ADP]/[TAN]) and ADP/ATP. *C*, isolated, intact hepatocyte respiratory states (routine, LEAK, and electron transport system) and flux control ratios: LEAK/routine (*L/R*), LEAK/electron transport system (*L/E*), and routine/electron transport system (*R/E*). *D*, schematic representation of select metabolites associated with NNMT-mediated transmethylation. *E*, NNMT-related metabolites: nicotinamide, 1-methylnicotinamide, nicotinamide mononucleotide, and NAD^+. Data are mean ± S.E. (*error bars*). $n = 6–9$ mice/group. *, $p < 0.05$ *versus* WT.

cosidase, an enzyme that hydrolyzes glycogen, in GNMT-null mice (25–27). Using $^2H/^{13}C$ MFA, a reduction in glycogenolysis (V_{PYGL}) was confirmed in KO mice.

Gluconeogenesis (V_{Enol}) was also reduced in KO mice. This impaired flux occurred in concert with a decline in liver gluconeogenic precursors. Gluconeogenesis is linked to the ability of substrates to enter and exit the CAC. Total cataplerosis (V_{PCK}) was lower in KO mice. Thus, reduced substrate exiting the CAC contributes to the lower gluconeogenesis and blood glucose. Under steady-state conditions, total cataplerosis and anaplerosis are balanced. As such, it is perhaps not surprising that entry of substrates into the CAC (V_{PCC} and V_{PC}) was reduced in KO mice. Factors that could slow anaplerotic flux include reductions in CAC fluxes, PC protein, and pyruvate as well as an increase in glutamate, an inhibitor of PC (28). Unlabeled anaplerotic substrate flux to pyruvate (V_{UAS}) was also lower in KO mice. A reduction in flux rates related to gluconeogenesis was associated with reduced amino acids that provide carbon for the CAC and gluconeogenesis.

Energy metabolism in livers of KO mice

Cataplerosis, anaplerosis, and CAC fluxes are intimately linked to energy metabolism. The NADH/NAD^+ ratio is a key regulator of CAC fluxes. NAD^+ was lower in the livers of KO mice. This is likely the result of an increase in NNMT function. Additionally, tryptophan, from which NAD^+ is also derived, was reduced in KO mice. Given that NAD^+ is used as a cofactor in CAC reactions, a lower NAD^+ availability would predictably diminish CAC flux. Notably, nicotinamide treatment prevents steatosis in GNMT KO mice (29). Restoration of NAD^+ homeostasis may assist in normalizing glucose and CAC-related metabolism in KO mice.

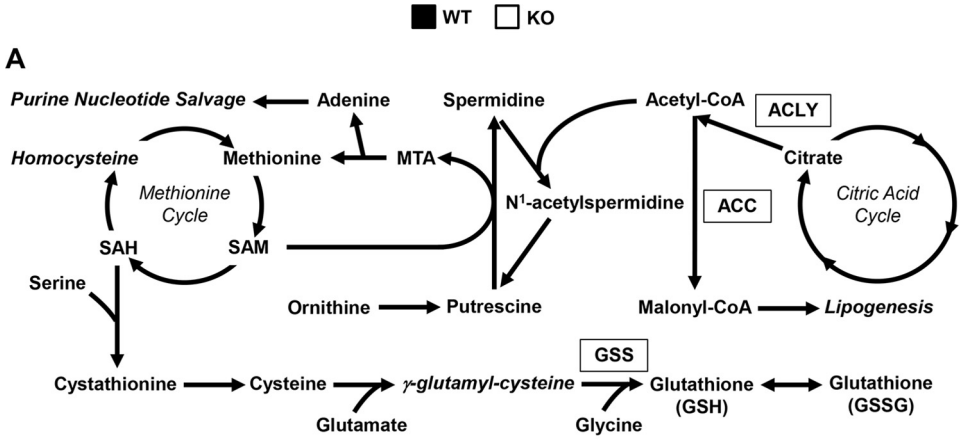

B

Pathway	Metabolite	KO/WT
Polyamine Metabolism	MTA	193.55*
	Ornithine	0.73*
	Putrescine	18.71*
	Spermidine	2.04*
	N^1-acetylspermidine	3.34*
	Adenine	7.46*
Fatty Acid Metabolism	Acetylcarnitine	1.02
	Malonylcarnitine	4.97*
Transsulfuration	Serine	0.62*
	Cystathionine	6.76*
	Cysteine	30.87*
Glutathione Metabolism	Glycine	0.84*
	GSH	151.12*
	GSSG	1.50*
	4-HNE	0.54
	GS-HNE	4.81*

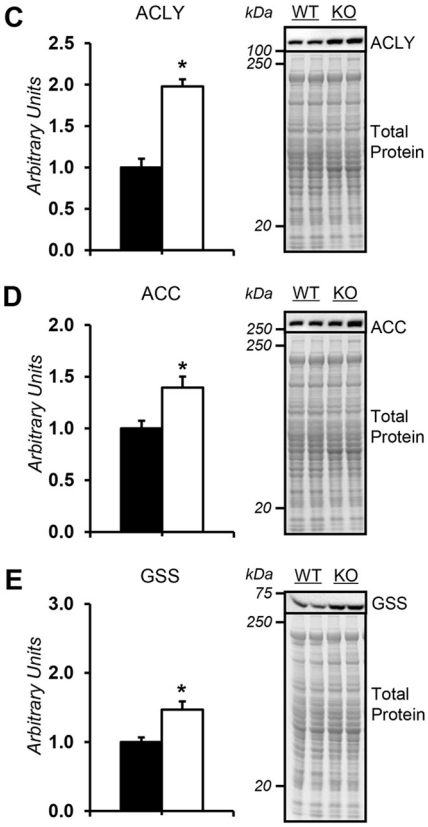

Figure 5. Alterations in liver SAM-consuming pathways in glycine *N*-methyltransferase knockout mice. *A*, *schematic representation* of select enzymes, metabolites, and pathways related to SAM homeostasis. *B*, liver metabolites related to SAM metabolism in glycine *N*-methyltransferase KO and WT mice: MTA, adenine, ornithine, putrescine, spermidine, N^1-acetylspermidine, acetylcarnitine, malonylcarnitine, serine, cystathionine, cysteine, glycine, GSH, GSSG, 4-hydroxy-2-nonenal (*4-HNE*), and 4-hydroxy-nonenal-GSH (*GS-HNE*). *C–E*, ACLY (*C*), ACC (*D*), and GSH synthetase (*GSS*) (*E*), as determined by immunoblotting and representative immunoblot. The total protein loading control image for ACLY is the same as that used for ACC, given that the immunoblots were performed on the same PVDF membrane. Data are mean ± S.E. (*error bars*). $n = 6–9$ mice/group. *, $p < 0.05$ *versus* WT.

In addition to redox state, hepatic adenine nucleotides in KO mice were characterized by a decrease in ATP and energy charge. This may reduce glucose production from CAC-derived substrates. Increases in ADP or the ADP/ATP ratio could inhibit pyruvate carboxylation (30, 31) and, subsequently, gluconeogenesis. Liver concentrations of ADP and the ADP/ATP ratio were increased ~3.5- and 4-fold, respectively, in KO mice. The pronounced increase in ADP/ATP ratio could be due to reduced hepatocyte oxygen consumption in KO mice. Moreover, LEAK as a fraction of routine respiration was higher in hepatocytes from KO mice. Thus, impaired and/or inefficient OXPHOS could contribute to the altered energy state.

SAM utilization pathways in KO mice

Pathways associated with liver SAM utilization were up-regulated. These pathways include transsulfuration and polyamine synthesis and breakdown (Fig. 6). The up-regulation of these pathways diverts carbons from CAC and gluconeogenic pathways.

Homocysteine enters the transsulfuration pathway rather than being remethylated to methionine due to SAM buildup in

Table 2
Hepatic acylcarnitine species and related metabolites
Data are mean ± S.E. for $n = 9$ mice/group. *, $p < 0.05$ between identified groups.

Acylcarnitines and related metabolites	KO	WT
Carnitine	1.53*	
Palmitoylcarnitine (C16)	0.44*	
Palmitoleoylcarnitine (C16:1)[a]	0.43*	
Stearoylcarnitine (C18)	0.83	
Linoleoylcarnitine (C18:2)[a]	0.28*	
Oleoylcarnitine (C18:1)	0.25*	
Arachidoylcarnitine (C20)[a]	0.33*	
Arachidonoylcarnitine (C20:4)	0.94	
Behenoylcarnitine (C22)[a]	0.52*	
Dihomolinolenoylcarnitine (20:3n3 or 6)[a]	1.09	
Eicosenoylcarnitine (C20:1)[a]	0.83	
Docosahexaenoylcarnitine (C22:6)[a]	0.80	
Lignoceroylcarnitine (C24)[a]	0.52*	
Margaroylcarnitine[a]	0.62*	

[a] Compounds that have not been officially confirmed based on a standard.

KO mice (Fig. 6). From a metabolic perspective, this is important because transsulfuration is linked to GSH synthesis (32, 33). Specifically, GSH is generated from cysteine via two reactions catalyzed by glutamate-cysteine ligase and GSS (32, 33). The increased glutamate-cysteine ligase reactants (glutamate and cysteine) and GSS protein promote the higher GSH. The formation of GSH diverts carbons (glutamate) away from the gluconeogenic pathway in KO mice. It is notable that the formation of GSH is elevated in human HCC (34).

The altered energy state of the liver in KO mice may be driven by SAM catabolism to adenine, as adenine salvage could increase adenine nucleotide pools (35, 36) (Fig. 6). SAM is catabolized to adenine through a series of reactions associated with polyamine synthesis (35, 36). Elevated intermediates of polyamine synthesis support the hypothesis that adenine salvage is increased in GNMT KO mice. SAM channeling to adenine nucleotides may link metabolic and cancer phenotypes. Polyamines are small polycations involved in cell growth and proliferation (9).

Polyamine concentrations influence nutrient handling via polyamine catabolism, which includes spermidine acetylation (22) (Fig. 6). The elevated N^1-acetylspermidine suggests that acetylation of polyamines is increased in KO mice. If N^1-acetylspermidine is used for putrescine resynthesis, a futile cycle utilizing acetyl-CoA ensues (22). Concurrently, KO mice displayed greater ACLY protein. We hypothesize that the metabolic changes in KO mice leading to lower gluconeogenesis from CAC intermediates and increased ACLY represent a coordinated attempt by the liver to reduce the elevated SAM via polyamine acetylation.

Liver steatosis in KO mice

The qualitative metabolomic data presented here suggest that elevated SAM and inhibition of gluconeogenesis facilitate triacylglyceride accumulation in KO mice (Fig. 6). Hepatic malonyl-carnitine, a reflection of malonyl-CoA, was elevated ~5-fold in KO mice. Malonyl-CoA attenuates the entry of long-chain fatty acids into the mitochondria, which limits provision of substrate for β-oxidation (37). In agreement, carnitine is elevated, and long-chain fatty acylcarnitines are reduced in livers from KO mice. The generation of malonyl-CoA involves the carboxylation of acetyl-CoA in a reaction mediated by ACC (37). ACC protein was greater in KO mice. Furthermore, citrate positively regulates ACC and may be used as a source for acetyl-CoA generation (37). It is reasonable to conclude that the metabolic mechanisms leading to increased citrate in livers of KO mice promote triacylglyceride accumulation by inhibiting β-oxidation. Malonyl-CoA is also substrate for fatty acid synthesis (37–39). Given that *de novo* lipogenesis is increased in cancer cells (40), one could propose that the shift in carbon flux away from gluconeogenesis to lipid synthesis is part of the metabolic reprogramming that supports tumorigenesis in KO mice.

SAM availability and metabolic reprogramming in KO mice

Whereas the metabolic alterations described in our studies focus on the mass action effects associated with increased SAM availability, additional mechanisms for the metabolic reprogramming should be considered. Cancer is often characterized by global DNA hypomethylation (41). KO mice displayed a decrease in 5-mC. Previous studies have reported that the reduced DNA methylation in GNMT-deficient mice is the result of lower DNA methyltransferase activity (17). Cancer cell DNA hypomethylation occurs in both repetitive elements and promoter regions of the genome (42). The general hypothesis is that DNA methylation acts to impede gene transcription (42). It is possible that the increase in hepatic ACLY, ACC, and GSS protein in KO mice may contribute to the extensive metabolic reprogramming. Ultimately, the elevated SAM resulting from GNMT deletion is associated with an elaborate metabolic reprogramming that involves multiple sites of regulation from gene to metabolite.

Conclusion

The results from this study demonstrate that GNMT-mediated transmethylation regulates glucose homeostasis. KO mice display reduced glucose production from glycogenolysis and gluconeogenesis and, subsequently, low blood glucose. In addition, KO mice are characterized by livers with impaired hepatic energy state, increased hepatic triglyceride levels, and greater GSH. This metabolic rewiring is associated with the increased SAM being utilized in lipogenic, polyamine, and transsulfuration pathways that also use gluconeogenic precursors. Of note, alterations in liver cell proliferation were not observed in KO mice in this study at 3 months of age. It is noteworthy that an increased proliferative phenotype is clearly evident after 8 months of age in GNMT-deficient mice (8, 18). Causality remains to be determined; however, we speculate that the increased SAM mediates metabolic reprogramming in KO mice that contributes to the eventual development of HCC.

Experimental procedures

Animal models

The Vanderbilt University Animal Care and Use Committee approved all procedures. Male mice with a whole-body KO of GNMT and WT littermates (43) were provided free access to food (PicoLab® Laboratory Rodent Diet 5L0D, Purina, Richmond, IN) and water. Mice were housed in a temperature- and humidity-controlled room on a 12/12-h light/dark cycle. All

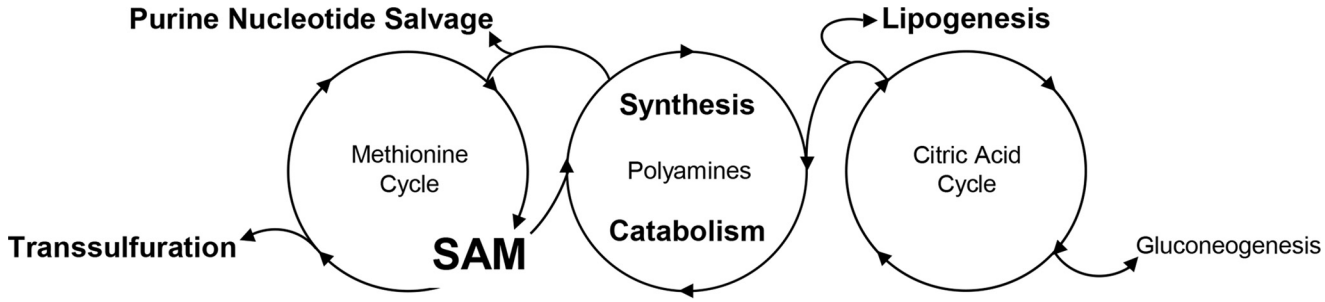

Figure 6. Schematic representation of metabolic reprogramming in glycine *N*-methyltransferase knockout mice. Glycine *N*-methyltransferase knockout (GNMT KO) mice exhibited a decline in gluconeogenesis. The changes in glucose metabolism were accompanied by an increase in lipid accumulation, polyamine synthesis and breakdown, and transsulfuration in KO mice. It is hypothesized that loss of GNMT results in metabolic reprogramming that redirects carbons from the gluconeogenic pathway to biosynthetic pathways that utilize SAM.

mice were studied at 3 months of age. Body composition was determined via an mq10 NMR analyzer (Bruker Corp., Billerica, MA).

Surgical procedures

At 11 weeks of age, catheterization procedures as previously performed (44) were completed on mice undergoing stable isotope infusions. Briefly, the carotid artery and jugular vein catheters were placed for arterial sampling and intravenous infusions, respectively. The free ends of the catheters were exteriorized behind the neck, flushed with 5 mg/ml ampicillin and 200 units/ml heparinized saline, and sealed with stainless steel plugs. Following surgery, the mice were housed individually and provided 7 days of postoperative recovery before stable isotope infusions.

Stable isotope infusions

See Fig. S1 for a schematic representation of the *in vivo* infusion procedures and time line. Food and water were withdrawn within 1 h of the start of the light cycle. The exteriorized catheters were connected to a two-channel swivel that was connected to infusion syringes 3 h into the fast. Following 1 h of acclimation, an 80-μl arterial blood sample was obtained to determine natural isotopic enrichment of plasma glucose. Venous infusions were performed as described previously (45). In brief, a ^2H_2O (99.9%)-saline bolus was administered over a 25-min period to enrich body water to 4.5%. [6,6-$^2H_2$]glucose (99%) was solubilized in the ^2H_2O-saline bolus for a prime (440 μmol·kg^{-1}). An independent, continuous [6,6-$^2H_2$]glucose (4.4 μmol·kg^{-1}·min^{-1}) infusion was initiated after the ^2H_2O-saline bolus and [6,6-$^2H_2$]glucose prime. A primed (1.1 mmol·kg^{-1}), continuous (0.055 mmol·kg^{-1}·min^{-1}) intravenous infusion of [$^{13}C_3$]propionate (99%, sodium salt) was started 2 h following the ^2H_2O bolus and [6,6-$^2H_2$]glucose prime. Four 100-μl arterial samples were obtained 90–120 min following the [$^{13}C_3$]propionate bolus (7.5–8 h of fasting) and stored at −20 °C. Mice were sacrificed by cervical dislocation. Excised tissues were freeze-clamped and stored at −80 °C. The 8-h time line was performed to quantify fluxes under conditions similar to prior studies reporting alterations in static metabolic characteristics in 8-h fasted GNMT-null mice (25). The stable isotopes were purchased from Cambridge Isotope Laboratories, Inc. (Tewksbury, MA). Each venous infusate was prepared in a 4.5% ^2H_2O-enriched saline solution unless otherwise specified.

$^2H/^{13}C$ metabolic flux analysis

Glucose derivatizations, GC-MS analysis, and MFA were completed using samples from 120 min before as well as 90, 100, and 110 min after the [$^{13}C_3$]propionate bolus, as outlined previously (46). Fragment ion ranges used for determining mass isotopomer distributions were as follows: aldonitrile, m/z 173–178, 259–266, 284–291, and 370–379; methyloxime, m/z 145–149; di-*O*-isopropylidene, m/z 301–314. Flux estimates for each sample were repeated 50 times from random initial values. Goodness of fit was accepted according to a χ^2 test ($p = 0.05$) with 34 degrees of freedom. Flux values for each mouse were an average of estimates obtained from samples at steady state (90, 100, and 110 min following the [$^{13}C_3$]propionate bolus). Multiple samples over time confirmed an isotopic steady state. Fluxes were normalized to liver weight.

Blood, plasma, and tissue analyses

Blood glucose was measured using an Accu-Chek® glucometer (Roche Diagnostics). Nonesterified fatty acids were measured in plasma obtained at the 100-min time point (7 h and 40 min of fasting) from mice undergoing the stable isotope infusions (NEFA C kit, Wako Chemicals USA Inc., Richmond, VA). Plasma insulin was measured as described previously (47) using plasma from the 120-min time point (8 h of fasting) of mice undergoing the stable isotope infusions. Plasma glucagon was assessed from the 120-min time point (8 h of fasting) of mice undergoing the stable isotope infusions using an ELISA (Mercodia Inc., Winston Salem, NC). Eight-hour-fasted, noncatheterized mice were sacrificed for analysis of liver metabolites, global DNA methylation, enzyme activities, and immunoblotting. The 8-h fast was chosen to match the time line of the flux studies. Samples were sent to Metabolon® (Metabolon Inc., Research Triangle Park, NC) for metabolite measurement as described previously (48). Hepatic glycogen, adenine nucleotides, phospholipids, and triacylglycerides were measured as outlined previously (48). According to the manufacturer's instructions, liver DNA was isolated using the DNeasy® blood and tissue kit (Qiagen, Germantown, MD), and 5-mC was measured via an ELISA (EpiGentek Group Inc., Farmingdale, NY; p-1030). Aminotransferase activity was measured using alanine transaminase (ab105134) and aspartate aminotransferase (ab105135) activity assay kits (Abcam, Cambridge, MA).

Immunoblotting

Liver tissue lysate was prepared as described previously (46). Liver (15–25 μg) proteins were denatured and reduced at 70 °C, separated on a NuPAGE 4–12% BisTris gel (Invitrogen), and transferred to a PVDF membrane. Membranes were probed with the following antibodies: ACC (Cell Signaling Technology (Danvers, MA), 3662, lot 4, 1:1000 dilution), ACLY (Thermo Fisher Scientific (Waltham, MA), PA5-29495, dilution 1:1000), GSS (ab91591 lot GR315302-4, dilution 1:1000), glycogen phosphorylase (PYGL; ab198268, lot GR216725-18, 1:1000 dilution), and PC (ab126707, lot GR95866-10, 1:1000 dilution) from Abcam (Cambridge, MA), GNMT (Santa Cruz Biotechnology, Inc., sc-68871, lot K0712, dilution 1:1000), and PEPCK (Cell Signaling Technology (Danvers, MA), 12940S; lot 1, 1:1000 dilution). Membranes were exposed to a chemiluminescent horseradish peroxidase substrate (MilliporeSigma) after incubating with a horseradish peroxidase–conjugated secondary antibody. A ChemiDoc™ imaging system and ImageLab™ software (Bio-Rad) were used to image the membranes. Total protein, determined via BLOT-FastStain (G-Bioscience, Geno Technology Inc., St. Louis, MO), was utilized as a loading control. ImageJ software was used for densitometry measurements.

Liver histology and immunohistochemistry

Liver tissue was fixed in zinc formalin (Thermo Fisher Scientific), paraffin-embedded, and sectioned (5 μm). For histology, Masson's trichrome blue staining was completed to provide a measurement of collagen. For immunohistochemistry, anti-Ki67 was used to assess cell proliferation. Histology and immunohistochemistry were performed by the Vanderbilt Translational Pathology Shared Resource. To quantify histological and immunohistochemical markers, whole-slide digital images (×20 magnification) were acquired using a Leica SCN400 slide scanner (Leica Microsystems, Buffalo Grove, IL). Quantification was performed using Leica SlidePath Digital Image Hub software (Leica Microsystems, Buffalo Grove, IL). Briefly, pixels of interest were selected manually to create a color definition file for each stain/antibody. The parameters of this file were subsequently applied to the entire tissue section. For Masson's trichrome blue stain, there were 2–3 liver sections per mouse. The measured stained area algorithm was used, and the percentage of stained area was calculated as 100× positive area/total tissue area. For Ki67, a single tissue section per mouse was analyzed to acquire the percentage of Ki67-positive nuclei using the measured stained cells algorithm.

Mouse hepatocyte isolation and high-resolution respirometry

Livers were perfused via the inferior vena cava with 50 ml of wash buffer (137 mM NaCl, 7 mM KCl, 0.7 mM $Na_2HPO_4 \cdot 12H_2O$, 10 mM Hepes, 50 mM EDTA, pH 7.65) followed by 50 ml of digestion buffer (wash buffer with 0.75 mg/ml $CaCl_2$ and 0.4 mg/ml collagenase) at 5 ml/min and 37 °C. Hepatocyte oxygen consumption was evaluated using an Oxygraph-2k (Oroboros Instruments Corp., Innsbruck, Austria) at 37 °C. Routine respiration was supported by DMEM (Gibco™, Thermo Fisher Scientific) containing 1125 mg/liter glucose and 584 mg/liter L-glutamine. Oligomycin (2.5 mM) assessed LEAK. ETS was determined via stepwise titrations (0.5 μM) of carbonyl cyanide-*p*-trifluoromethoxyphenylhydrazone.

Statistical analyses

Student's *t* tests or two-way repeated measures analysis of variance to detect statistical differences ($p < 0.05$) followed by Bonferroni post hoc tests were performed using SigmaStat® software (Systat Software Inc., San Jose, CA). All data are reported as means ± S.E.

Author contributions—C. C. H. and D. H. W. contributed to the conception and design of experiments. C. C. H., E. T., F. D. J., D. P. B., and E. P. D. contributed to data acquisition. C. C. H. analyzed and interpreted data. C. C. H. drafted the manuscript. All authors contributed to revising the manuscript for critically important intellectual content. All authors approved the manuscript for publication.

Acknowledgments—We thank the Vanderbilt University Mouse Metabolic Phenotyping Center Analytical Core Services (National Institutes of Health Grants DK059637 and DK020593). Whole-slide imaging was performed by the Digital Histology Shared Resource at Vanderbilt University Medical Center.

References

1. Forner, A., Reig, M., and Bruix, J. (2018) Hepatocellular carcinoma. *Lancet* **391,** 1301–1314 CrossRef Medline
2. Bellentani, S. (2017) The epidemiology of non-alcoholic fatty liver disease. *Liver Int.* **37,** 81–84 CrossRef Medline
3. Younossi, Z. M., Otgonsuren, M., Henry, L., Venkatesan, C., Mishra, A., Erario, M., and Hunt, S. (2015) Association of nonalcoholic fatty liver disease (NAFLD) with hepatocellular carcinoma (HCC) in the United States from 2004 to 2009. *Hepatology* **62,** 1723–1730 CrossRef Medline
4. Martínez-Una, M., Varela-Rey, M., Mestre, D., Fernandez-Ares, L., Fresnedo, O., Fernández-Ramos, D., Gutiérrez-de Juan, V., Martin-Guerrero, I., García-Orad, A., Luka, Z., Wagner, C., Lu, S. C., García-Monzon, C., Finnell, R. H., Aurrekoetxea, I., *et al.* (2015) *S*-Adenosylmethionine increases circulating very-low density lipoprotein clearance in non-alcoholic fatty liver disease. *J. Hepatol.* **62,** 673–681 CrossRef Medline
5. Liao, Y. J., Chen, T. L., Lee, T. S., Wang, H. A., Wang, C. K., Liao, L. Y., Liu, R. S., Huang, S. F., and Chen, Y. M. (2012) Glycine *N*-methyltransferase deficiency affects Niemann-Pick type C2 protein stability and regulates hepatic cholesterol homeostasis. *Mol. Med.* **18,** 412–422 Medline
6. Chen, Y. M., Shiu, J. Y., Tzeng, S. J., Shih, L. S., Chen, Y. J., Lui, W. Y., and Chen, P. H. (1998) Characterization of glycine-*N*-methyltransferase-gene expression in human hepatocellular carcinoma. *Int. J. Cancer* **75,** 787–793 CrossRef Medline
7. Avila, M. A., Berasain, C., Torres, L., Martín-Duce, A., Corrales, F. J., Yang, H., Prieto, J., Lu, S. C., Caballería, J., Rodés, J., and Mato, J. M. (2000) Reduced mRNA abundance of the main enzymes involved in methionine metabolism in human liver cirrhosis and hepatocellular carcinoma. *J. Hepatol.* **33,** 907–914 CrossRef Medline
8. Martínez-Chantar, M. L., Vázquez-Chantada, M., Ariz, U., Martínez, N., Varela, M., Luka, Z., Capdevila, A., Rodríguez, J., Aransay, A. M., Matthiesen, R., Yang, H., Calvisi, D. F., Esteller, M., Fraga, M., Lu, S. C., *et al.* (2008) Loss of the glycine *N*-methyltransferase gene leads to steatosis and hepatocellular carcinoma in mice. *Hepatology* **47,** 1191–1199 Medline
9. Lu, S. C., and Mato, J. M. (2012) *S*-Adenosylmethionine in liver health, injury, and cancer. *Physiol. Rev.* **92,** 1515–1542 CrossRef Medline
10. DeBerardinis, R. J., and Chandel, N. S. (2016) Fundamentals of cancer metabolism. *Sci. Adv.* **2,** e1600200 CrossRef Medline
11. Lunt, S. Y., and Vander Heiden, M. G. (2011) Aerobic glycolysis: meeting the metabolic requirements of cell proliferation. *Annu. Rev. Cell Dev. Biol.* **27,** 441–464 CrossRef Medline

12. Savic, L. J., Chapiro, J., Duwe, G., and Geschwind, J. F. (2016) Targeting glucose metabolism in cancer: new class of agents for loco-regional and systemic therapy of liver cancer and beyond? *Hepat. Oncol.* **3,** 19–28 CrossRef Medline
13. Shang, R. Z., Qu, S. B., and Wang, D. S. (2016) Reprogramming of glucose metabolism in hepatocellular carcinoma: Progress and prospects. *World J. Gastroenterol.* **22,** 9933–9943 CrossRef Medline
14. Chen, M., Zhang, J., Li, N., Qian, Z., Zhu, M., Li, Q., Zheng, J., Wang, X., and Shi, G. (2011) Promoter hypermethylation mediated downregulation of FBP1 in human hepatocellular carcinoma and colon cancer. *PLoS One* **6,** e25564 CrossRef Medline
15. Yeo, E. J., and Wagner, C. (1994) Tissue distribution of glycine *N*-methyltransferase, a major folate-binding protein of liver. *Proc. Natl. Acad. Sci. U.S.A.* **91,** 210–214 CrossRef Medline
16. Jacobs, R. L., Stead, L. M., Brosnan, M. E., and Brosnan, J. T. (2001) Hyperglucagonemia in rats results in decreased plasma homocysteine and increased flux through the transsulfuration pathway in liver. *J. Biol. Chem.* **276,** 43740–43747 CrossRef Medline
17. Liao, Y. J., Liu, S. P., Lee, C. M., Yen, C. H., Chuang, P. C., Chen, C. Y., Tsai, T. F., Huang, S. F., Lee, Y. H., and Chen, Y. M. (2009) Characterization of a glycine *N*-methyltransferase gene knockout mouse model for hepatocellular carcinoma: implications of the gender disparity in liver cancer susceptibility. *Int. J. Cancer* **124,** 816–826 CrossRef Medline
18. Liu, S. P., Li, Y. S., Lee, C. M., Yen, C. H., Liao, Y. J., Huang, S. F., Chien, C. H., and Chen, Y. M. (2011) Higher susceptibility to aflatoxin B(1)-related hepatocellular carcinoma in glycine *N*-methyltransferase knockout mice. *Int. J. Cancer* **128,** 511–523 CrossRef Medline
19. Brosnan, M. E., and Brosnan, J. T. (2009) Hepatic glutamate metabolism: a tale of 2 hepatocytes. *Am. J. Clin. Nutr.* **90,** 857S–861S CrossRef Medline
20. Hems, R., Ross, B. D., Berry, M. N., and Krebs, H. A. (1966) Gluconeogenesis in the perfused rat liver. *Biochem. J.* **101,** 284–292 CrossRef Medline
21. Martínez-Uña, M., Varela-Rey, M., Cano, A., Fernández-Ares, L., Beraza, N., Aurrekoetxea, I., Martínez-Arranz, I., García-Rodríguez, J. L., Buqué, X., Mestre, D., Luka, Z., Wagner, C., Alonso, C., Finnell, R. H., Lu, S. C., Martínez-Chantar, M. L., *et al.* (2013) Excess *S*-adenosylmethionine reroutes phosphatidylethanolamine towards phosphatidylcholine and triglyceride synthesis. *Hepatology* **58,** 1296–1305 CrossRef Medline
22. Pegg, A. E. (2008) Spermidine/spermine-N^1-acetyltransferase: a key metabolic regulator. *Am. J. Physiol. Endocrinol Metab.* **294,** E995–E1010 CrossRef Medline
23. Hirata, H., Sugimachi, K., Komatsu, H., Ueda, M., Masuda, T., Uchi, R., Sakimura, S., Nambara, S., Saito, T., Shinden, Y., Iguchi, T., Eguchi, H., Ito, S., Terashima, K., Sakamoto, K., *et al.* (2016) Decreased expression of fructose-1,6-bisphosphatase associates with glucose metabolism and tumor progression in hepatocellular carcinoma. *Cancer Res.* **76,** 3265–3276 CrossRef Medline
24. Ma, R., Zhang, W., Tang, K., Zhang, H., Zhang, Y., Li, D., Li, Y., Xu, P., Luo, S., Cai, W., Ji, T., Katirai, F., Ye, D., and Huang, B. (2013) Switch of glycolysis to gluconeogenesis by dexamethasone for treatment of hepatocarcinoma. *Nat. Commun.* **4,** 2508 CrossRef Medline
25. Liu, S. P., Li, Y. S., Chen, Y. J., Chiang, E. P., Li, A. F., Lee, Y. H., Tsai, T. F., Hsiao, M., Huang, S. F., and Chen, Y. M. (2007) Glycine *N*-methyltransferase−/− mice develop chronic hepatitis and glycogen storage disease in the liver. *Hepatology* **46,** 1413–1425 CrossRef Medline
26. Zubiete-Franco, I., García-Rodríguez, J. L., Martínez-Uña, M., Martínez-Lopez, N., Woodhoo, A., Juan, V. G., Beraza, N., Lage-Medina, S., Andrade, F., Fernandez, M. L., Aldámiz-Echevarría, L., Fernández-Ramos, D., Falcon-Perez, J. M., Lopitz-Otsoa, F., Fernandez-Tussy, P., *et al.* (2016) Methionine and *S*-adenosylmethionine levels are critical regulators of PP2A activity modulating lipophagy during steatosis. *J. Hepatol.* **64,** 409–418 CrossRef Medline
27. Adeva-Andany, M. M., González-Lucán, M., Donapetry-García, C., Fernández-Fernández, C., and Ameneiros-Rodríguez, E. (2016) Glycogen metabolism in humans. *BBA Clin.* **5,** 85–100 CrossRef Medline
28. Scrutton, M. C., and White, M. D. (1974) Pyruvate carboxylase: inhibition of the mammalian and avian liver enzymes by α-ketoglutarate and L-glutamate. *J. Biol. Chem.* **249,** 5405–5415 Medline
29. Varela-Rey, M., Martínez-López, N., Fernández-Ramos, D., Embade, N., Calvisi, D. F., Woodhoo, A., Rodríguez, J., Fraga, M. F., Julve, J., Rodríguez-Millán, E., Frades, I., Torres, L., Luka, Z., Wagner, C., Esteller, M., Lu, S. C., Martínez-Chantar, M. L., and Mato, J. M. (2010) Fatty liver and fibrosis in glycine N-methyltransferase knockout mice is prevented by nicotinamide. *Hepatology* **52,** 105–114 CrossRef Medline
30. von Glutz, G., and Walter, P. (1976) Regulation of pyruvate carboxylation by acetyl-CoA in rat liver mitochondria. *FEBS Lett.* **72,** 299–303 CrossRef Medline
31. Keech, D. B., and Utter, M. F. (1963) Pyruvate Carboxylase. Ii. Properties. *J. Biol. Chem.* **238,** 2609–2614 Medline
32. Lu, S. C. (2009) Regulation of glutathione synthesis. *Mol. Aspects Med.* **30,** 42–59 CrossRef Medline
33. Lu, S. C. (2013) Glutathione synthesis. *Biochim. Biophys. Acta* **1830,** 3143–3153 CrossRef Medline
34. Huang, Z. Z., Chen, C., Zeng, Z., Yang, H., Oh, J., Chen, L., and Lu, S. C. (2001) Mechanism and significance of increased glutathione level in human hepatocellular carcinoma and liver regeneration. *FASEB J.* **15,** 19–21 CrossRef Medline
35. Avila, M. A., García-Trevijano, E. R., Lu, S. C., Corrales, F. J., and Mato, J. M. (2004) Methylthioadenosine. *Int. J. Biochem. Cell Biol.* **36,** 2125–2130 CrossRef Medline
36. Savarese, T. M., Crabtree, G. W., and Parks, R. E., Jr. (1981) 5′-Methylthioadenosine phosphorylase-L: substrate activity of 5′-deoxyadenosine with the enzyme from Sarcoma 180 cells. *Biochem. Pharmacol.* **30,** 189–199 CrossRef Medline
37. Foster, D. W. (2004) The role of the carnitine system in human metabolism. *Ann. N.Y. Acad. Sci.* **1033,** 1–16 CrossRef Medline
38. Foster, D. W. (2012) Malonyl-CoA: the regulator of fatty acid synthesis and oxidation. *J. Clin. Invest.* **122,** 1958–1959 CrossRef Medline
39. McGarry, J. D., Takabayashi, Y., and Foster, D. W. (1978) The role of malonyl-CoA in the coordination of fatty acid synthesis and oxidation in isolated rat hepatocytes. *J. Biol. Chem.* **253,** 8294–8300 Medline
40. Mounier, C., Bouraoui, L., and Rassart, E. (2014) Lipogenesis in cancer progression (review). *Int. J. Oncol.* **45,** 485–492 CrossRef Medline
41. Ehrlich, M. (2009) DNA hypomethylation in cancer cells. *Epigenomics* **1,** 239–259 CrossRef Medline
42. Long, M. D., Smiraglia, D. J., and Campbell, M. J. (2017) The genomic impact of DNA CpG methylation on gene expression: relationships in prostate cancer. *Biomolecules* **7,** E15 Medline
43. Luka, Z., Capdevila, A., Mato, J. M., and Wagner, C. (2006) A glycine *N*-methyltransferase knockout mouse model for humans with deficiency of this enzyme. *Transgenic Res.* **15,** 393–397 CrossRef Medline
44. Ayala, J. E., Bracy, D. P., Malabanan, C., James, F. D., Ansari, T., Fueger, P. T., McGuinness, O. P., and Wasserman, D. H. (2011) Hyperinsulinemic-euglycemic clamps in conscious, unrestrained mice. *J. Vis. Exp.* CrossRef Medline
45. Hasenour, C. M., Wall, M. L., Ridley, D. E., Hughey, C. C., James, F. D., Wasserman, D. H., and Young, J. D. (2015) Mass spectrometry-based microassay of ^2H and ^{13}C plasma glucose labeling to quantify liver metabolic fluxes *in vivo*. *Am. J. Physiol. Endocrinol. Metab.* **309,** E191–E203 CrossRef Medline
46. Hughey, C. C., James, F. D., Bracy, D. P., Donahue, E. P., Young, J. D., Viollet, B., Foretz, M., and Wasserman, D. H. (2017) Loss of hepatic AMP-activated protein kinase impedes the rate of glycogenolysis but not gluconeogenic fluxes in exercising mice. *J. Biol. Chem.* **292,** 20125–20140 CrossRef Medline
47. Morgan, C. R., and Lazarow, A. (1965) Immunoassay of pancreatic and plasma insulin following alloxan injection of rats. *Diabetes* **14,** 669–671 CrossRef Medline
48. Hasenour, C. M., Ridley, D. E., James, F. D., Hughey, C. C., Donahue, E. P., Viollet, B., Foretz, M., Young, J. D., and Wasserman, D. H. (2017) Liver AMP-activated protein kinase is unnecessary for gluconeogenesis but protects energy state during nutrient deprivation. *PLoS One* **12,** e0170382 CrossRef Medline